Deformation and Failure Behavior of Woven Composite Laminates

M. Karayaka
Visiting Research Associate.

P. Kurath
Director.

Advanced Materials Testing and Evaluation Laboratory,
University of Illinois at Urbana-Champaign,
100K Talbot Lab., 104 S. Wright,
Urbana, IL 61801

Conceptually, fabric composites have some structural advantages over conventional laminates. However, deformation and failure analyses become more complex with the additional anisotropy introduced by the weaving geometry. A micromechanistic deformation model, that could realistically be incorporated into structural finite element codes, is proposed where loading direction and weave parameters are allowed to vary. Comparisons are made to previous models and experimental results for woven materials, indicating that the proposed model provides improved estimates for the linear elastic stiffness. The model further provides predictions for internal stresses in the longitudinal, transverse, and interlace regions of the woven laminate which qualitatively correspond to the experimentally observed failure mechanisms. The experimental program investigates deformations behavior and failure mechanisms of 5-harness 0/90 weave Graphite/Epoxy laminates under tension, compression, and 3-point and 4-point bending loading. Under these conditions the woven laminates exhibit orientation dependent mechanical properties and strength.

1 Introduction

Presently, woven fabrics are being considered as alternatives to unidirectional prepregs in the manufacturing of composite laminates. Weaving provides a network of reinforcing fibers in the through-the-thickness direction that improves the interlaminar shear strength and impact resistance of those planes susceptible to delamination. Although woven laminates possess more balanced properties than their unidirectional counterparts, geometrical and material imperfections such as fiber misalignment, fiber clustering, and fiber and ply waviness inherently introduced in the laminate microstructure may significantly alter the mechanical behavior and failure mechanisms. Failure mechanisms of woven laminates are often associated with these micro- and macro-level inhomogeneities and currently are not well identified. There is a critical need for deformation models and experimental studies that address the effects of weaving geometry on mechanical behavior and failure mechanisms of woven composite laminates. This study presents a systematic experimental and theoretical study on the deformation and failure behavior of woven composite laminates.

To date, continuum mechanics models proposed for evaluating the macroscopic behavior of composite laminates often follow a direct approach involving three steps: 1) selection of a representative volume to homogenize the structure of the composite medium, 2) selection of boundary conditions which satisfy equilibrium and compatibility conditions, and 3) integration of state variables to obtain effective properties. In this study a direct approach is also adopted to investigate the elastic deformation behavior of woven composite laminates.

Although the selection of a representative volume is a standard procedure for modelling unidirectional laminates (Chou et al., 1972; Pagano, 1974; Postma, 1955; Sun, 1988; 1990), it is a tedious task for woven laminates due to their high anisotropy at several structural levels. Ishikawa, Chou and co-workers have proposed several homogenization procedures for woven composite laminates in their mosaic (Ishikawa, 1981; 1983), fiber undulation (Ishikawa, 1982a; 1982b), bridging (Ishikawa, 1982b), and fiber inclination (Ishikawa, 1982a; Yang, 1986) models. Naik and co-workers (1992a,b; Shembekar, 1992) have developed highly detailed slice array and element array models for plain-weave laminates. These homogenization procedures, with the exception of the mosaic model, take into account the fiber continuity and fiber waviness at the interlaced regions. Homogenization procedures proposed for the more complicated microstructures of multidimensionally braided composites include use of the braiding parameters and yarn properties (Ko, 1986; Byun, 1990, 1991; Du, 1991).

Various forms of boundary conditions for the homogenized medium have been selected in the literature. The assumption of uniform strain and uniform stress states in the selected representative volume, as adopted in the mosaic model, leads to upper and lower bounds predictions for the effective properties. A more common approach, which satisfies equilibrium and compatibility conditions, is the selection of either a uniform strain or a uniform stress state for different planes of the laminate. This mixed boundary condition, first proposed by Postma (1955) for thick laminates, assumes uniform normal and shear stress states in the thickness direction and uniform normal and shear strain states in the laminate plane. Several deformation models have used these mixed boundary conditions to predict the effective properties of thick classical laminates (Chou, 1972; Sun, 1988, 1990).

Contributed by the Materials Division for publication in the JOURNAL OF ENGINEERING MATERIALS AND TECHNOLOGY. Manuscript received by the Materials Division March 12, 1993. Associate Technical Editor: D. Hui.

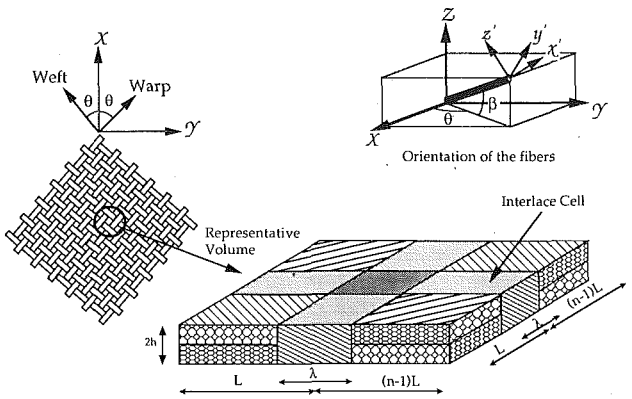

Fig. 1 Schematics of homogenization procedure for woven composite laminates

2 Modeling

2.1 Homogenization Procedure. Woven fabrics are formed by interlacing two sets of yarns. The angle between these yarns, also called warp and weft yarns, and the density of the interlacing defines the weaving geometry. A three-dimensional representative volume is considered for modeling the deformation behavior of woven composite laminates. The geometry of woven fabric is characterized by the angle between the warp and weft yarns, 2θ, repeat of the interlaced regions, n, and the length of the interlaced region, λ. These weaving parameters and the selected representative volume element are schematically illustrated in Fig. 1. Note that the representative volume corresponds to plain-weave laminates for $n=2$ and to classical laminates for $n=\infty$. The principal reference frame is set up such that the longitudinal and transverse loading directions, X and Y axes, are in the lamina plane, and the Z axis is in the thickness direction of the lamina. The properties associated with the X-Y plane will be referred to as in-plane properties, and properties associated with the thickness direction will be referred to as out-of-plane properties.

The representative volume is made of cells with unidirectional reinforcement. The mechanical properties of these cells may differ depending on the warp and weft yarn properties. The orientation of the fibers in these cells about the principal reference frame is schematically illustrated in Fig. 1. The in-plane orientation of the fibers, the angle between the loading direction and warp and weft directions, is indicated by angle θ. The out-of-plane inclination of the fibers in the interlaced region is indicated by angle β. The linear elastic deformation behavior of the cell in the local reference frame $x'y'z'$ is governed by:

$$\begin{Bmatrix}\sigma_{x'x'}\\ \sigma_{y'y'}\\ \sigma_{z'z'}\\ \tau_{y'z'}\\ \tau_{x'z'}\\ \tau_{x'y'}\end{Bmatrix}=\begin{bmatrix}C_{11}&C_{12}&C_{13}&0&0&0\\ C_{21}&C_{22}&C_{23}&0&0&0\\ C_{31}&C_{32}&C_{33}&0&0&0\\ 0&0&0&C_{44}&0&0\\ 0&0&0&0&C_{55}&0\\ 0&0&0&0&0&C_{66}\end{bmatrix}\begin{Bmatrix}\epsilon_{x'x'}\\ \epsilon_{y'y'}\\ \epsilon_{z'z'}\\ \gamma_{y'z'}\\ \gamma_{x'z'}\\ \gamma_{x'y'}\end{Bmatrix} \quad (1)$$

In this representation the fibers are aligned in the x' direction, and in-plane and out-of-plane strains are not coupled. A constitutive equation of each cell relating stresses and strains in the principal coordinate system XYZ can be calculated by performing tensor transformations (see, Love, 1944). Linear elastic deformation of a cell, which involves both the in-plane and out-of-plane orientation of fibers, is governed by the following constitutive equation:

$$\begin{Bmatrix}\sigma_{XX}\\ \sigma_{YY}\\ \sigma_{ZZ}\\ \tau_{YZ}\\ \tau_{XZ}\\ \tau_{XY}\end{Bmatrix}=\begin{bmatrix}C_{11}&C_{12}&C_{13}&C_{14}&C_{15}&C_{16}\\ C_{21}&C_{22}&C_{23}&C_{24}&C_{25}&C_{26}\\ C_{31}&C_{32}&C_{33}&C_{34}&C_{35}&C_{36}\\ C_{41}&C_{42}&C_{43}&C_{44}&C_{45}&C_{46}\\ C_{51}&C_{52}&C_{53}&C_{54}&C_{55}&C_{56}\\ C_{61}&C_{62}&C_{63}&C_{64}&C_{65}&C_{66}\end{bmatrix}\begin{Bmatrix}\epsilon_{XX}\\ \epsilon_{YY}\\ \epsilon_{ZZ}\\ \gamma_{YZ}\\ \gamma_{XZ}\\ \gamma_{XY}\end{Bmatrix} \quad (2)$$

For classical laminates, in which only the in-plane orientation of fibers is involved, the equivalent stiffness tensor may assume special forms. A critical evaluation of these special forms is given by Christensen (1988). For woven composites we will use the general form of the stiffness tensor given in Eq. (2). This equation is partitioned into its in-plane and out-of-plane components.

In-plane stresses:

$$\begin{Bmatrix}\sigma_{XX}\\ \sigma_{YY}\\ \tau_{XY}\end{Bmatrix}=\begin{bmatrix}C_{11}&C_{12}&C_{16}\\ C_{21}&C_{22}&C_{26}\\ C_{61}&C_{62}&C_{66}\end{bmatrix}\begin{Bmatrix}\epsilon_{XX}\\ \epsilon_{YY}\\ \gamma_{XY}\end{Bmatrix}+\begin{bmatrix}C_{13}&C_{14}&C_{15}\\ C_{23}&C_{24}&C_{25}\\ C_{63}&C_{64}&C_{65}\end{bmatrix}\begin{Bmatrix}\epsilon_{ZZ}\\ \gamma_{XZ}\\ \gamma_{YZ}\end{Bmatrix} \quad (3)$$

Out-of-plane stresses:

$$\begin{Bmatrix}\sigma_{ZZ}\\ \tau_{XZ}\\ \tau_{YZ}\end{Bmatrix}=\begin{bmatrix}C_{31}&C_{32}&C_{36}\\ C_{41}&C_{42}&C_{46}\\ C_{51}&C_{52}&C_{56}\end{bmatrix}\begin{Bmatrix}\epsilon_{XX}\\ \epsilon_{YY}\\ \gamma_{XY}\end{Bmatrix}+\begin{bmatrix}C_{33}&C_{34}&C_{35}\\ C_{43}&C_{44}&C_{45}\\ C_{53}&C_{54}&C_{55}\end{bmatrix}\begin{Bmatrix}\epsilon_{ZZ}\\ \gamma_{XZ}\\ \gamma_{YZ}\end{Bmatrix} \quad (4)$$

Subsequently, the following nomenclature will be employed to represent Eqs. (3) and (4), respectively:

$$\sigma_{in}=C_1\epsilon_{in}+C_2\epsilon_{out} \quad (5)$$

$$\sigma_{out}=C_3\epsilon_{in}+C_4\epsilon_{out} \quad (6)$$

In this representation subscripts "$_{in}$" and "$_{out}$" indicate in-plane and out-of-plane properties, respectively. As defined in Eqs. (3) and (4), C_1, C_2, C_3, and C_4 are 3×3 matrices, and σ_{in}, σ_{out}, ϵ_{in}, and ϵ_{out} are 3×1 vectors.

2.2 Effective Properties. A direct approach is implemented in computing the effective properties of the representative volume described in Section 2.1. Effective stress, $\bar{\sigma}_i$, and effective strain, $\bar{\epsilon}_i$, are defined as volumetric averages of local stresses, σ_i, and local strains, ϵ_i:

$$\bar{\epsilon}_i=\frac{1}{V}\int_V \epsilon_i\,dV \qquad i=1,2,\ldots.6 \quad (7)$$

and

$$\bar{\sigma}_i=\frac{1}{V}\int_V \sigma_i\,dV \qquad i=1,2,\ldots.6 \quad (8)$$

For elastic deformations, average stresses and average strains are related through effective stiffness $\bar{C}_{ij}$:

$$\bar{\sigma}_i=\bar{C}_{ij}\bar{\epsilon}_j \qquad i,j=1,2,\ldots.6 \quad (9)$$

The evaluation of volumetric integrals 7 and 8 requires determination of stress and strain fields within the representative volume. In this study, uniform stress and strain distributions in each cell are assumed. We further assume the following stress and displacement continuity conditions at the interface of each cell:

$$\bar{\epsilon}_{in} = \epsilon_{in}^k \qquad k = 1, \ldots N \tag{10.1}$$

$$\bar{\sigma}_{out} = \sigma_{out}^k \qquad k = 1, \ldots N \tag{10.2}$$

where N is the number of cells in the representative volume.

Combining the boundary conditions (Eqs. (10.1), (10.2)) and volumetric integrals (Eqs. (7), (8)) describes a complete boundary value problem which predicts effective properties of the representative volume. First, Eqs. (5) and (6) are rearranged to express out-of-plane strains and in-plane stresses in terms of in-plane strains and out-of-plane stresses.

$$\sigma_{in} = (C_1 - C_2 C_4^{-1} C_3)\epsilon_{in} + C_2 C_4^{-1}\sigma_{out} \tag{11}$$

$$\epsilon_{out} = C_4^{-1}\sigma_{out} - C_4^{-1} C_3 \epsilon_{in} \tag{12}$$

Next, by using the boundary conditions given in Eq. (10), the volumetric integrals 7 and 8 are evaluated to calculate effective in-plane stresses and out-of-plane strains

$$\bar{\sigma}_{in} = C_1^* \bar{\epsilon}_{in} + C_2^* \bar{\sigma}_{out} \tag{13}$$

$$\bar{\epsilon}_{out} = C_3^* \bar{\sigma}_{out} - C_4^* \bar{\epsilon}_{in} \tag{14}$$

where

$$C_1^* = \sum_{k=1}^{N} f_k (C_1 - C_2 C_4^{-1} C_3)^k \tag{15.1}$$

$$C_2^* = \sum_{k=1}^{N} f_k (C_2 C_4^{-1})^k \tag{15.2}$$

$$C_3^* = \sum_{k=1}^{N} f_k (C_4^{-1})^k \tag{15.3}$$

$$C_4^* = \sum_{k=1}^{N} f_k (C_4^{-1} C_3)^k \tag{15.4}$$

where f_k is the volume fraction of the kth cell in the representative volume.

The effective stiffness tensor, $\bar{C}_{ij}$, of the representative volume is constructed by concatenating matrices C_1^*, C_2^*, C_3^*, and C_4^*:

$$\bar{\sigma}_{out} = C_3^{*-1} C_4^* \bar{\epsilon}_{in} + C_3^{*-1} \bar{\epsilon}_{out}$$

$$\bar{\sigma}_{in} = (C_1^* + C_2^* C_3^{*-1} C_4^*)\bar{\epsilon}_{in} + C_2^* C_3^{*-1} \bar{\epsilon}_{out} \tag{16}$$

Remotely applied stresses are selected as the loading parameters. Constitutive equations (Eqs. (16)) which describe global deformation behavior of the laminate are used to predict in-plane and out-of-plane strains. The localized deformation behavior of the warp, weft, and interlace regions of the laminate are calculated using Eqs. (11) and (12). This approach gives a description of average micro- and macro-level deformation behaviors of the laminate for a given loading condition. Since warp, weft, and interlace regions of the laminate microstructure exhibit distinctly different material properties, localized deformation histories of these regions differ from the global behavior.

Next, the effective property predictions are used with the well-established classical lamination theory to characterize mechanical behavior of thin woven composite laminates. In this case, the boundary condition 10.1 is modified to:

$$\bar{\epsilon}_{in} = = \epsilon_{in}^k + z\kappa_{in}^k \qquad k = 1, \ldots N \tag{17}$$

This boundary condition implies that, both in-plane strains, ϵ_{in}^k, and in-plane curvatures, κ_{in}^k, (mid-laminate strains and curvatures) are constant in the representative volume. Based on stress equilibrium and compatibility conditions, the constitutive equation for a laminate which contains m layers with thickness h_m is given by (see, Jones, 1975):

Table 1 Summary of weave parameters for 5-harness satin 0/90 weave IM7/8551 7A graphite/epoxy laminates

Weave density	$n = 5$	Laminate thickness	3 mm
Tow width	$L = 3$ mm	Ply thickness	$h = 0.33$ mm
Interlace length	$\lambda = 6.75$ mm	Interlace parameter	$\lambda^* = 0.45$

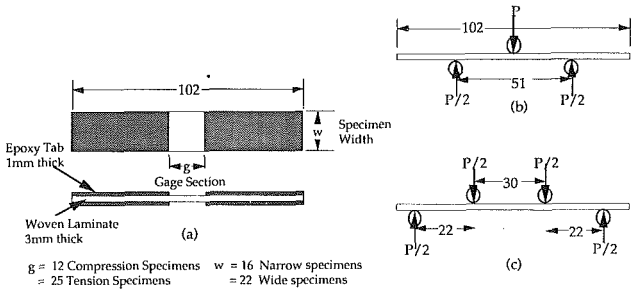

Fig. 2 Specimen geometry, (*a*) tension and compression, (*b*) 3-pt bending, (*c*) 4-pt bending

$$\begin{Bmatrix} N_i \\ M_i \end{Bmatrix} = \begin{bmatrix} A_{ij} & B_{ij} \\ B_{ij} & D_{ij} \end{bmatrix} \begin{Bmatrix} \epsilon_j \\ \kappa_j \end{Bmatrix} \tag{18}$$

where,

$$(A_{ij}, B_{ij}, D_{ij}) = \sum_{k=1}^{m} \times ((h_k - h_{k-1}),\ (h_k^2 - h_{k-1}^2)/2,\ (h_k^3 - h_{k-1}^3)/3) Q_{ij}^k$$

In this equation N_i and M_i are the resultant forces and moments acting on laminate, ϵ_i is the in-plane strains, and κ_i is the in-plane curvature of the laminate. The macromechanical behavior of composite laminates is characterized by extensional stiffness, A_{ij}, coupling stiffness, B_{ij}, and bending stiffness, D_{ij}.

Based on the plane stress assumption, the stiffness tensor of the woven laminate, Q_{ij}, is equal to the weighed average of C_1 given in Eq. (5). In developing deformation models for woven composites, however, using the plane stress assumption may not account for the contribution of out-of-plane inclination of fibers at the interlaced regions. In the ensuing simulations, therefore, the reduced stiffness given by C_1^* (Eq. (15.1)) is used for Q_{ij}.

3 Material, Test Equipment, and Experimental Procedure

Monotonic tension, compression, three-point bending, and four-point bending experiments are conducted on 5-harness satin 0/90 weave IM7/8551-7A Graphite/Epoxy laminates. The weaving parameters of the laminates and the material properties for the tows are summarized in Table 1 and Table 2, respectively. The specimens are cut from a 12 × 12 in. square 9-ply laminate along the warp and weft directions (0/90 specimens) and along the 45 deg off-axes direction (−45/45 specimens). Specimen dimensions are indicated in Fig. 2. The tension and compression specimens are tabbed utilizing a 1 mm thick epoxy sheet. The gage length of the tension and compression specimens is 25 mm and 12 mm, respectively. The specimen width is 22 mm for all of the experiments with the exception of the compression experiments, which are duplicated with narrow specimens.

The compression experiments are conducted utilizing an IITRI test fixture. Dimensions of the three-point and four-point bending fixtures are indicated in Figs. 2(*b*) and 2(*c*). Note that the three-point bending specimens have a depth to span ratio of 1:16. During tension experiments, longitudinal and transverse strains are measured with a biaxial extensometer. For the compression and bending experiments, strain gages

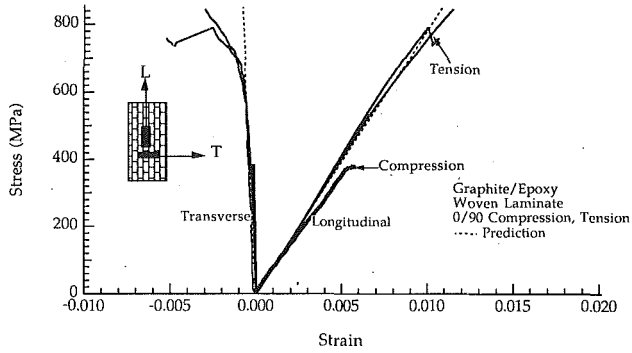

Fig. 3(*a*)

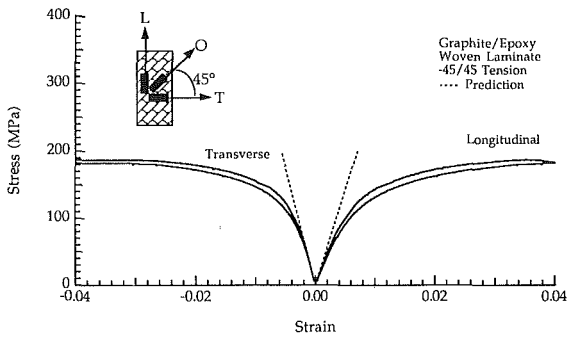

Fig. 3(*b*)

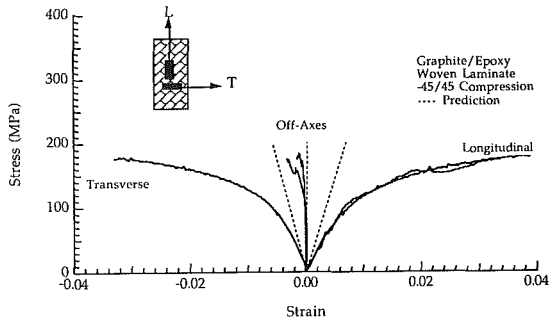

Fig. 3(*c*)

Fig. 3 Stress-strain behavior of (*a*) 0/90 specimens under tension and compression, (*b*) −45/45 specimens under tension, (*c*) −45/45 specimens under compression

are placed along the longitudinal, transverse, and 45 deg off-axes directions. Width and length of the strain gages are 3 mm and 6 mm, respectively.

4 Results

4.1 Experiments and Predictions. Figures 3 and 4 present experimental and predicted longitudinal, transverse, and off-axes strain-stress behavior of the 0/90 and −45/45 specimens under tension, compression, and bending conditions. The longitudinal and transverse strains are indicated by L and T, respectively. In some of the experiments, as indicated by O in the inset, the 45 deg off-axes strains are also reported. Elastic properties and strength of the woven laminates are found to be highly dependent on the specimen orientation. The 0/90 specimens exhibit linear stress-strain behavior until they break catastrophically. The specimens loaded in the off-axes direction exhibit nonlinear stress-strain behavior. The compressive strength (380 MPa) of the 0/90 specimens is found to be 55 percent lower than their tensile strength (840 MPa). Under off-axes loading conditions the compressive strength (0.2 percent

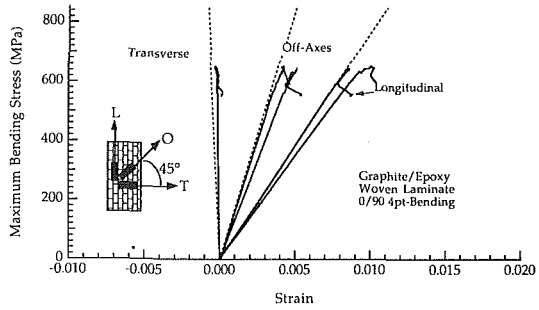

Fig. 4(*a*)

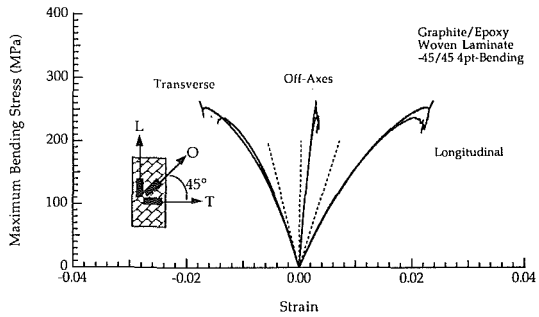

Fig. 4(*b*)

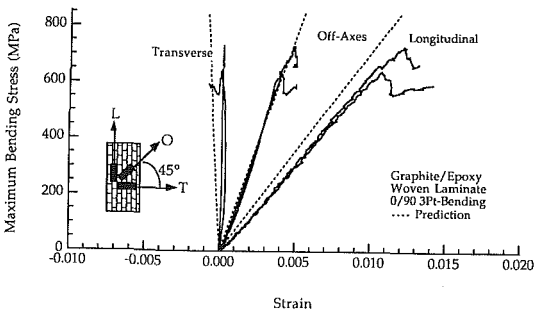

Fig. 4(*c*)

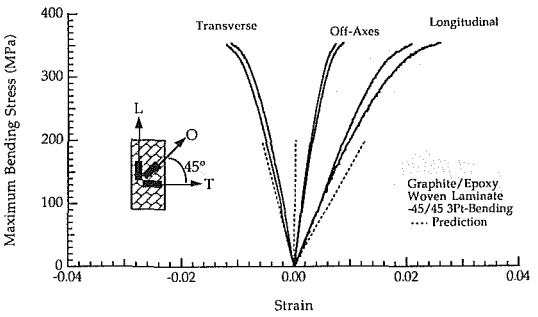

Fig. 4(*d*)

Fig. 4 Stress-strain behavior at the tensile surface of (*a*) 0/90 specimens under 4-Point bending loading, (*b*) −45/45 specimens under 4-Point bending loading, (*c*) 0/90 specimens under 3-Point bending loading, (*d*) −45/45 specimens under 3-Point bending loading

off-set) of the 0/90 specimens is 25 percent lower than the tensile strength.

The elastic property predictions closely follow the experimental results for the 0/90 specimens. Stress-strain behavior of the −45/45 specimens is closely predicted at the initial stages of deformation. However, due to nonlinear composite behavior, predictions deviate from the experimental results at high strain levels. Predicted and experimentally observed elastic properties of the 5-harness satin IM7/8551-7A are summarized

Table 2 Mechanical properties for the tows (Agarwal and Broutman, 1990)

Elastic constants		Strengths	
Longitudinal modulus	$E_L = 203$ (GPa)	Tensile longitudinal	$\sigma_L = 3500$ (MPa)
Transverse modulus	$E_T = 11.2$ (GPa)	Tensile transverse	$\sigma_T = 56$ (MPa)
Shear modulus	$G_{LT} = 8.4$ (GPa)	Compressive longitudinal	$\sigma_{l_c} = 1540$ (MPa)
In-plane Poisson's ratio	$\nu_{LT} = 0.32$	Compressive transverse	$\sigma_T = 150$ (MPa)
Out-of-plane Poisson's ratio	$\nu_{TT} = 0.3$	Shear	$\tau_{LT} = 98$ (MPa)

Table 3 Mechanical properties of 5-harness satin IM7/8551-7A graphite/epoxy woven laminates

0/90 Loading orientation			
	Tensile	Compression	Prediction
Modulus (GPa)	81	76	78
Poisson's ratio	0.063	0.056	0.073

−45/45 Loading orientation				
	Tensile	Compression (Wide)	Compression (Narrow)	Prediction
Modulus (GPa)	22	19	16	28
Poisson's ratio	0.67	0.73	0.70	0.65

in Table 3. Gage and width lengths of the specimens considered in this study are in the order of size of the repeating unit cells of 5-harness satin laminates which may lead to scatter in the experimental observations. However, duplicate experiments in each loading condition resulted in consistent stress-strain response and elastic property measurements (Figs. 3, 4). The effect of specimen size on mechanical behavior is studied only for compression loading conditions. Elastic modulus of the narrow specimens is slightly lower than that of the wider specimens.

Effective properties of the woven laminates are compared to those of the cross-ply laminates in Fig. 5. Cross-ply laminate simulations ($n = \infty$) are indicated by dashed lines, and woven laminate simulations ($n = 5$) are indicated by solid lines. The woven laminates exhibit lower modulus compared to that of the cross-ply laminates. For small off-axes loading angles, cross-ply laminates exhibit an effective longitudinal modulus as much as 35 percent higher than that of the woven laminates. For larger off-axis angles, however, the contribution of out-of-plane reinforcement to the in-plane properties decreases and predictions of the effective longitudinal moduli for both cross-ply laminates and woven laminates become very close.

The effective properties of the woven laminates are sensitive to both interlace length and loading angle. Figure 6 presents a parametric study on the contribution of interlace length to longitudinal modulus predictions for the 0/90 and −45/45 specimens. The predictions are normalized by corresponding experimental values. An interlace parameter, λ^*, is defined as:

$$\lambda^* = \frac{\lambda}{nL} \tag{19}$$

The interlace parameter is also a measure of out-of-plane inclination of the yarns. Microscopic observations indicated that the characteristic interlace parameter is 0.45 for the 5-harness satin graphite/epoxy laminate considered in this study. The left side of the Fig. 6 corresponds to fabric with no interlace yarns, which also resembles Chou's mosaic model. The right side of the figure corresponds to fabric without straight regions (fully inclined). The longitudinal modulus prediction for the 0/90 laminate deviates by as much as 30 percent from the experimental data. Stiffness predictions for the off-axes specimens exhibits less sensitivity to the interlace parameter. The deviation of longitudinal modulus predictions from the experimental data is minimal for interlace parameter values greater than 0.4. Since denser weaving (e.g., $n < 5$) results in frequent out-of-plane orientation of the yarns at the interlace

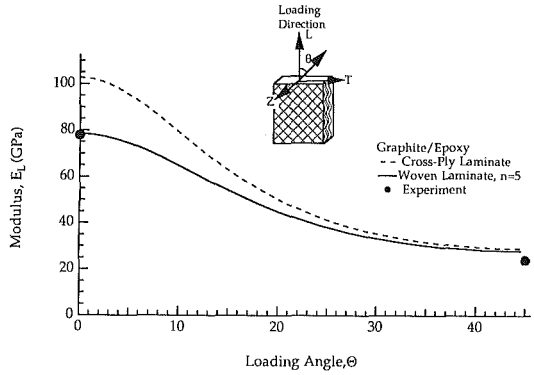

Fig. 5 Effective property simulations for classical and woven laminates

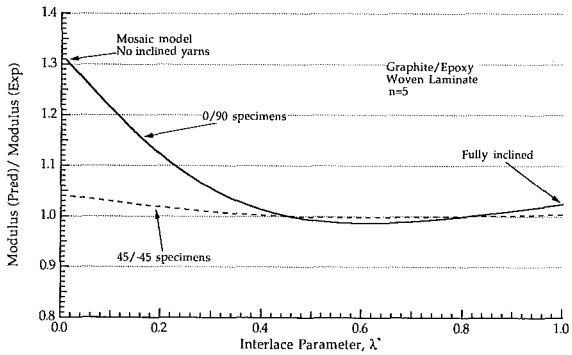

Fig. 6 Contribution of interlace length on the effective properties of woven laminates

regions, the effective properties of these laminates are more sensitive to the interlace parameter.

4.2 Microscopic Observations. Failure mechanisms of 0/90 and −45/45 specimens observed under tension, compression, and bending conditions are schematically illustrated in Fig. 7. The failure modes of the woven laminates are often governed by several competing micro-failure mechanisms. Failure of the −45/45 specimens involves accumulation of damage under tension, compression, and bending loading conditions. Matrix microcracking may lead to nonlinear stress-strain behavior of the laminates under off-axes loading conditions. Under off-axes loading conditions, interaction of several failure mechanisms results in a loss of stiffness and leads to failure whereas the failure of 0/90 specimens is catastrophic and is governed by a primary failure mechanism.

Tensile and compressive failures of the −45/45 laminates involve damage accumulation in the matrix followed by fiber (yarn) failure and ply delamination. Microscopic observation on tension and compression −45/45 specimens indicates a network of matrix microcracks running along the fiber direction (Figs. 8, 9). Propagation of these microcracks in the transverse direction follows two patterns under tensile loading conditions. When fibers of the facing plies run in different directions the transverse crack propagation stops at the delaminated interface. When the facing plies have the same fiber

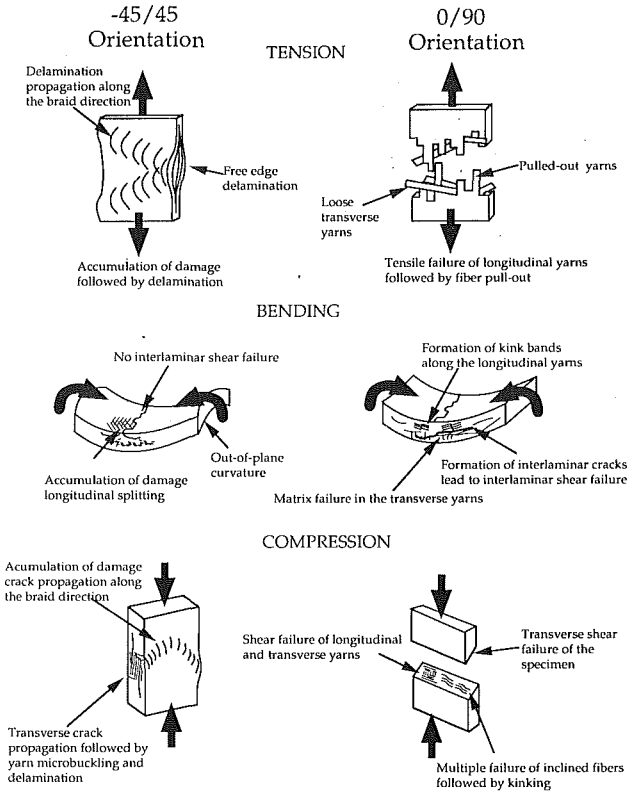

Fig. 7 Failure mechanisms of woven composite laminates

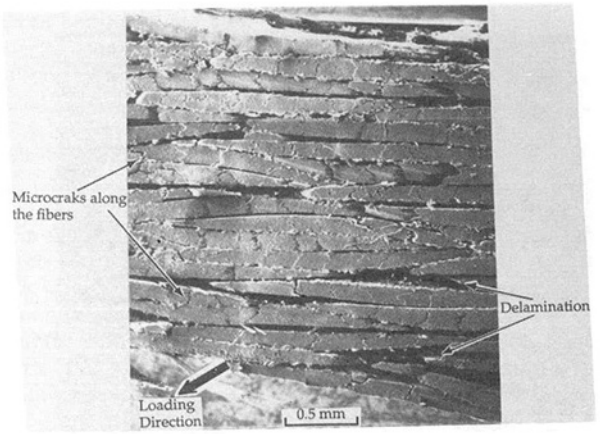

Fig. 8 Network of transverse microcracks running along the fiber directions and delamination. Horizontal cross-section of −45/45 specimens loaded in tension.

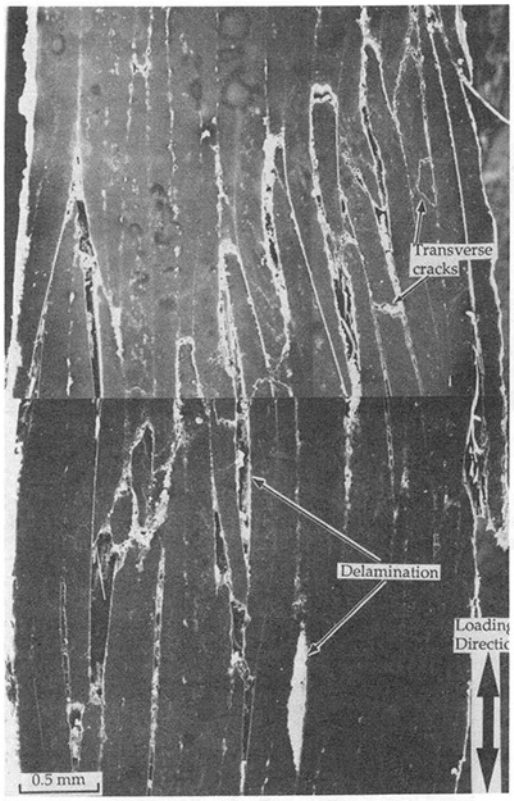

Fig. 9 Transverse microcracks and yarn micro-buckling. Longitudinal cross-section of −45/45 specimens loaded in compression.

direction, microcracks transversely propagate through the individual laminates and delaminated interfaces, which indicates that delamination occurs during the later stages of failure. Delamination of the plies starts at the free edge and propagates as a band along the weave directions (Fig. 7). Under compressive loading, damage accumulation in the matrix is followed by buckling of yarns in the transverse direction (Fig. 9). Buckling of the yarns is promoted at the interlace regions, which the fibers are inclined in the out-of-plane direction. Analogous to observations for tensile loading, delamination propagation of the compression specimens also follows the weave direction.

Figure 10 shows micrographs of the 0/90 and −45/45 specimens tested under the three-point bending loading condition. The view is the long edge of the specimen with the bottom of the micrograph representing the tensile edge and the top of the micrograph representing the compressive stress edge. Under bending loading conditions there is a competition among tensile, compressive, and shear failure mechanisms. Stresses at the outer layer of the −45/45 specimens are greater than both the tensile and compressive strengths (Figs. 3, 4). This indicates that tensile and compressive damage accumulates at the outer layers, while the inner layers are able to sustain the interlaminar shear stresses (Fig. 10(*b*)). The three-point bending specimens, in which only the strain gage location is subjected to the maximum stresses, exhibit higher stresses than the four-point bending specimens, in which a span of the laminate is subjected to the maximum stresses. The accumulation of damage in the four-point bending specimens is, therefore, likely to occur over a larger portion of the specimen than for the three-point bending specimens and results in lower stresses.

The 0/90 specimens exhibit linear stress-strain behavior similar under both three-point and four-point bending. Failure of the 0/90 specimens is governed by interlaminar shear (Fig. 10(*a*)). The flexure strength of 0/90 specimens is 700 MPa, which is greater than their compressive strength and less than their tensile strength, therefore, compressive damage at the outer layer is expected. Kink failure and propagation along the longitudinal yarns is observed at the compression side of the specimen (Fig. 11). Note that the kinked longitudinal yarn makes an angle with the longitudinal direction. Inclination of the longitudinal yarns in the out-of-plane direction promotes fiber microbuckling under compressive loading conditions. The micrograph given in Fig. 12 shows microcracks formed at the compressive side of a −45/45 bending specimen. The matrix microcracks avoid fiber fracture, propagate in the transverse direction of the laminate, and join the interlaminar microcracks. Note that the transverse microcracks do not propagate through the laminates because fibers of the neighboring laminates run in different directions. The failure mechanisms under bending loading conditions are summarized in Fig. 7.

Tensile and compressive failure mechanisms of the 0/90

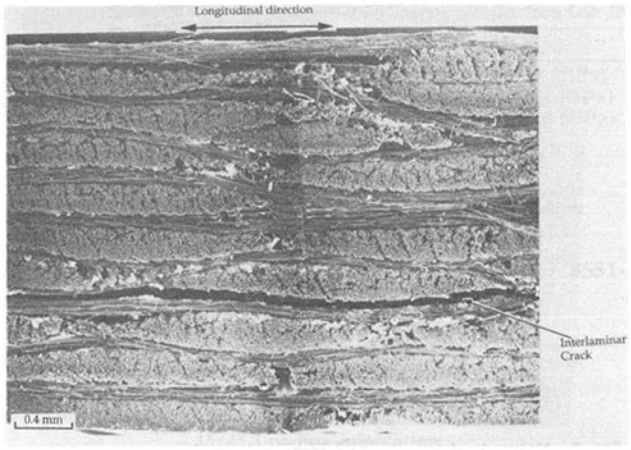

Fig. 10(*a*)

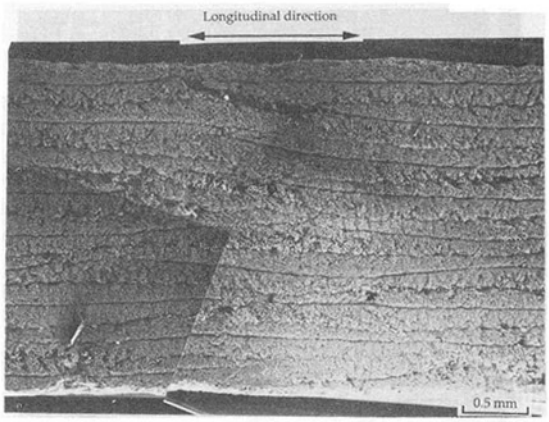

Fig. 10(*b*)

Fig. 10 Bending failure of (*a*) 0/90 and (*b*) −45/45 specimens. Top and bottom layers of the laminate correspond to compression and tension regions, respectively.

Fig. 11 Kink failure of longitudinal fibers at the compressive region of the 0/90 laminate during bending

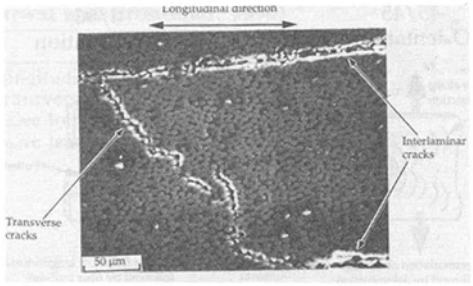

Fig. 12 Transverse and interlaminar microcracks at the tensile region of the −45/45 laminate during bending

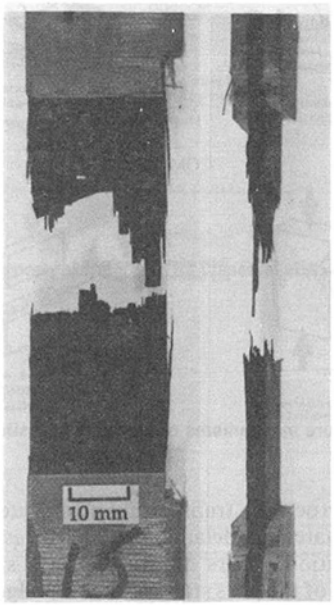

Fig. 13 Tensile failure of 0/90 specimens

specimens are distinctly different from those of the −45/45 specimens. While damage accumulation in the form of matrix microcracking and propagation leads to the failure of −45/45 specimens, failure of the 0/90 specimens is predominantly governed by failure of the longitudinal yarns. Under tensile loading the longitudinal yarns are fractured perpendicular to the loading direction and pulled out from the matrix (Fig. 13). The fracture surface also exhibits loose transverse yarns which carry an insignificant load compared to the longitudinal yarns.

Under compressive loading conditions the 0/90 specimens fail due to transverse shear. The fracture surface makes a 25 deg angle with the loading direction. Locally, the transverse and longitudinal yarns exhibit distinctly different fracture surface morphologies which indicates that several localized failure mechanisms lead to transverse shear failure of the laminate. Propagation of the major crack in the matrix without fracturing transverse fibers leads to a smooth fracture surface for the transverse yarns. Compressive failure of the longitudinal yarns is due to microbuckling of the fibers in the out-of-plane direction. Figures 14 and 15 show a typical fracture surface morphology of longitudinal and longitudinally inclined regions, respectively. The fracture surface of the longitudinal yarns consists of tiered regions. The smooth fracture surface of the large tiered regions suggests that local crack propagation occurs in a cooperative manner for the longitudinal fibers. Rough and small tiered regions of the longitudinally inclined fibers indicate that failure is due to an accumulation process. Out-of-plane inclination of the longitudinal fibers promotes multiple fracture of the fibers.

4.3 Parametric Studies on Effective Properties. Early deformation models for woven composites considered uniform strain, $\bar{\epsilon}_i = \epsilon_i^k$, and uniform stress, $\bar{\sigma}_i = \sigma_i^k$, boundary conditions in the representative volumes to establish upper and lower bounds for the effective properties. In current representation, these boundary conditions lead to:

$$\bar{C}_{ij} = \sum_{k=1}^{N} f_k C_{ij}^k, \qquad \bar{C}_{ij}^{-1} = \sum_{k=1}^{N} f_k C_{ij}^{-1k} \tag{20}$$

for upper and lower bounds of effective stiffness, respectively. The stiffness tensor, C_{ij}^k, of each cell in the representative volume is given in Eq. (2).

The variation of extensional stiffness, A_{11}, and coupling stiffness, B_{11}, (normalized by their counterparts for cross-ply laminates) with regard to 1/n is illustrated in Figs. 16 and 17. The dashed lines indicate upper and lower boundary predictions, and the dark solid lines indicate simulations based on boundary conditions given by Eqs. (10.2) and (17). The left side of these figures corresponds to cross-ply laminates and the right side to plain-weave laminates. The simulations demonstrate that both extensional and coupling stiffnesses of the woven laminates are lower than those of the cross-ply laminates. Extensional stiffness predictions for the plain-weave composites are 40 percent lower than that of the classical laminates. The coupling stiffness, which implies interaction between the bending and extension of a laminate, vanishes for plain-weave laminates.

A comparative study of the current deformation models for woven composite laminates is illustrated in Fig. 16. The change of in-plane stiffness of the woven laminates with interlace density is closely predicted. The differences between these models arise due to the choice of homogenization procedures and boundary conditions. All of the experimental data and simulations, with the exception of the upper bound of the mosaic model, fall within the upper and lower bounds obtained by assuming uniform stress and uniform strain in the represent-

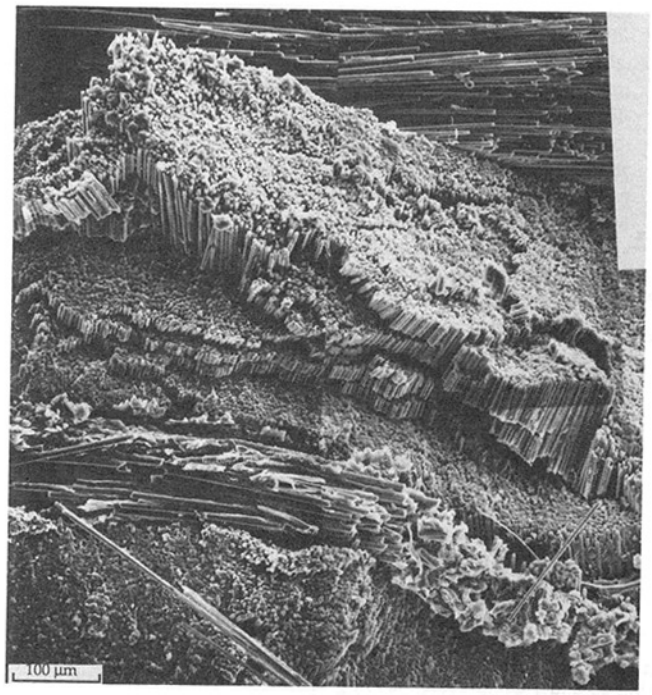

Fig. 14 Fracture surface morphology of 0/90 specimens loaded in compression, longitudinally inclined fiber region

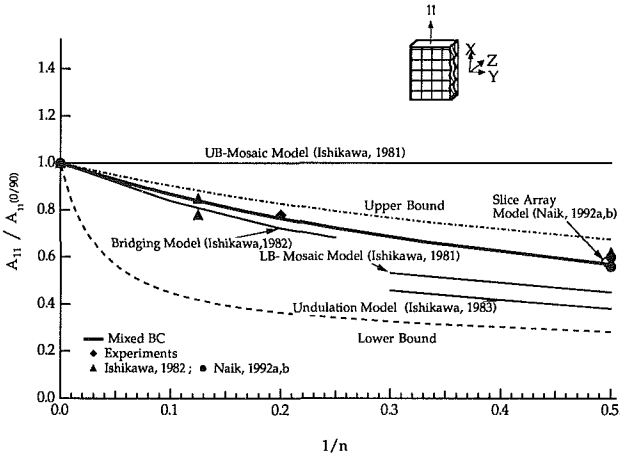

Fig. 16 Compression of effective in-plane stiffness, A11, predictions with mosaic, fiber undulation, bridging, and slice array models

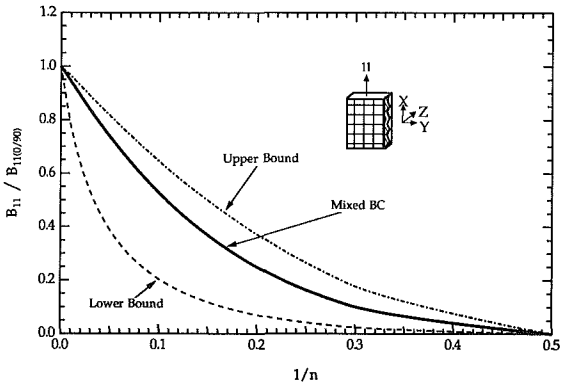

Fig. 17 Variation of effective coupling stiffness, B11, regarding to 1/n

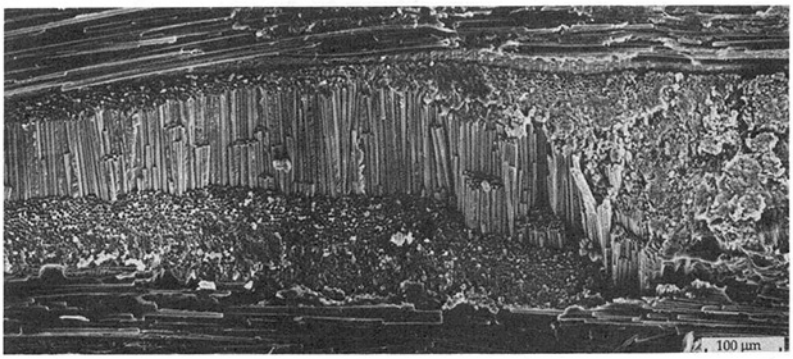

Fig. 15 Fracture surface morphology of 0/90 specimens loaded in compression, longitudinal fiber region

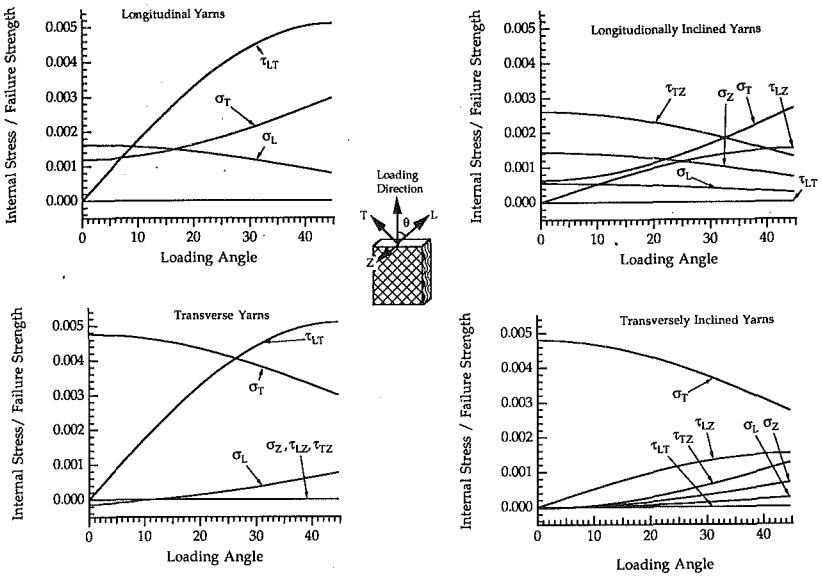

Fig. 18 Internal stresses in longitudinal, transverse, and interlace regions of the woven composite laminates under tensile loading

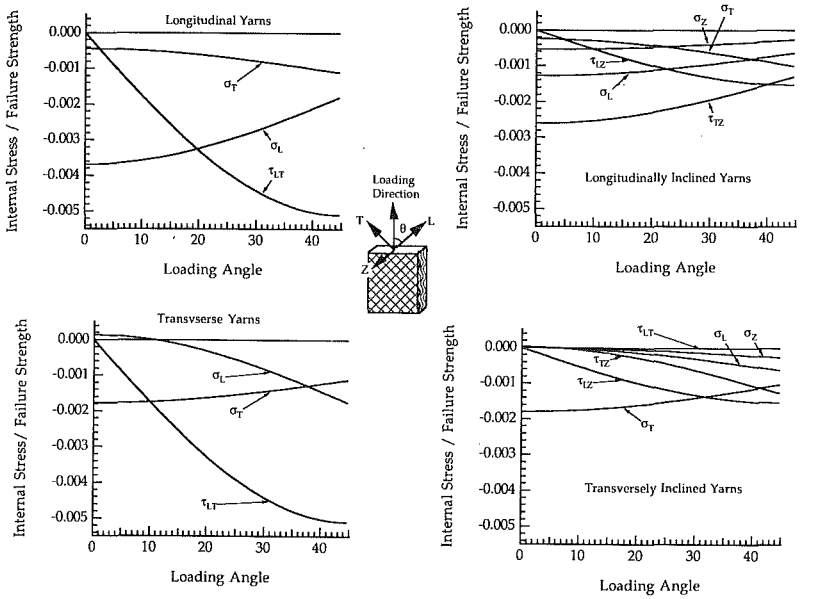

Fig. 19 Internal stresses in longitudinal, transverse, and interlace regions of the woven composite laminates under compression loading

ative volume (Eq. (20)). The mosaic, undulation, and bridging models, which follow the plane stress assumption of the classical lamination theory, neglect the contributions of through-the-thickness reinforcement on effective properties. The homogenization procedure implemented in the bridging model assumes uniform in-plane strain distribution in the interlace region and uniform stress distribution in the cross-ply regions. These conditions are similar to the mixed boundary conditions presented in Eqs. (10(*a*)) and (10(*b*)). Therefore, the predictions of the bridging model and our model are similar. Naik's (1992*a*, *b*) and Shembekar (1992) experimental data and predictions for plain-weave laminates also agree with the current deformation model.

Mirzadeh and Reifsnider (1992) have reported on extensive finite element and Moiré interferometry studies on in-plane strain distributions in eight-harness satin laminates. As expected, imperfections in the composite microstructure have resulted in non-uniform global distribution of in-plane stresses and strains. However, locally, Moiré interferometry measurements have indicated a uniform in-plane strain distribution along the thickness of laminate. Furthermore, the out-of-plane stresses under uniaxial loading conditions are generally zero for the regions away from the free edges of the laminates. These observations serve as an experimental verification for the use of boundary conditions 10*a* and 10*b*/17 to characterize deformation of woven laminates at the onset of localized failure.

4.4 Internal Deformation Behavior. Figures 18 and 19 present internal stress predictions in the longitudinal, transverse and interlace regions of the woven laminate under uniaxial loading conditions. In these simulations the laminate is subjected to unit remote stress of ±1 MPa. The global stress-strain behavior is calculated by the constitutive equations (Eq. (16)) developed in the previous section. After prediction of the global deformation, internal stress-strain behaviors of the lon-

gitudinal, transverse, and interlace regions are calculated by using Eqs. (13) and (14). Tensor transformations are then performed to calculate, longitudinal (fiber direction, indicated by subscript L) and transverse stress (in-plane, indicated by subscript T, and out-of-plane, indicated by subscript Z) components in each region. In order to compare the relative contributions of internal stresses to failure, the internal stresses are normalized by the corresponding failure strength of a unidirectional laminate (Table 2). Longitudinal stresses are normalized by longitudinal failure strength, transverse stresses are normalized by transverse failure strength, and so on. The purpose of these simulations is to gain insight into the variation of internal stresses with the loading direction for a woven laminate with perpendicular warp and weft yarns. The left side of the figures (0 deg loading angle) corresponds to 0/90 specimens and the right side of the figures (45 deg loading angle) corresponds to $-45/45$ laminates.

Some of the experimentally observed micro- and macro-failure mechanisms and failure modes are attributed to internal stresses developed in the longitudinal, transverse, and interlace regions of the laminate. The predictions reveal that a multitude of competing damage mechanisms due to longitudinal, in-plane transverse, and out-of-plane stresses may be operative for a given loading direction. The predominant failure mechanism and location vary with the loading angle. Failure of the longitudinal and transverse yarns is governed by in-plane stresses. For both tensile and compressive loading, a transition from longitudinal to shear failure and from transverse to shear failure is predicted for longitudinal and transverse yarns, respectively. The stress state at the interlace regions is further complicated due to the out-of-plane inclination of fibers. The out-of-plane stresses contribute not only to in-plane failure mechanisms such as fiber microbuckling, longitudinal splitting, and kinking, but may also initiate ply delamination.

Under tensile loading conditions the transverse and transversely inclined yarns appear to be the regions most likely to initiate laminate failure. Failure of the transverse yarns is governed by tensile transverse stresses for small loading angles and by in-plane shear stresses for large loading angles. However, transverse yarns of the 0/90 specimens carry only 10 percent of the applied load. Therefore, early failure of the transverse yarns does not significantly contribute to laminate failure for small off-axes loading conditions. Failure of the 0/90 laminates is governed by longitudinal failure of the longitudinal yarns, which conforms with the experimentally observed fiber failure and fiber pull-out mechanisms (Fig. 13).

As the loading angle increases, the longitudinal and transverse yarns sustain a comparable portion of the applied load, which leads to uniform damage development in the laminate. For example, the transverse and longitudinal yarns of the $-45/45$ specimens experience identical stress state due to their symmetry with respect to the loading direction. Microscopic observations on these specimens indicate delamination along the weave direction and a uniform network of longitudinal cracks running along the fiber direction (Fig. 8). The in-plane shear and tensile transverse stresses predicted in the laminate microstructure may lead to initiation and propagation of matrix microcracks and promote fiber splitting. Also note that the out-of-plane stresses, maximum at 45 deg for off-axes loading, contribute to delamination initiation and propagation at the interlace regions.

Orientation of fibers with respect to loading direction plays a significant role in compressive strength and associated failure mechanisms. Under compressive loading conditions the longitudinal and longitudinally inclined yarns appear to be the regions most likely to initiate failure of the laminate. Microscopic observations on the fracture surface of the 0/90 specimens indicate that the longitudinal fibers buckle in the transverse direction and fail in flexure (Figs. 14, 15). While the longitudinal and transverse yarns exhibit a smooth fracture surface, the inclined fibers are fractured at several locations. The out-of-plane stresses predicted in the longitudinally inclined regions may promote fiber micro-buckling and result in multiple failure of the off-axes fibers. Like tensile loading, uniform stress distribution in the transverse and longitudinal yarns leads to a uniform compressive damage accumulation for off-axes loading conditions. The $-45/45$ specimens exhibit a network of cracks running along the warp and the yarns (Fig. 9).

5 Conclusions

This study presents a preliminary experimental and theoretical investigation of the deformation and failure mechanisms of woven composite laminates for tensile, compressive, and bending loading conditions. The experimental observations indicate that numerous failure mechanisms and failure modes are operative for different laminate orientations. The micromechanical deformation model provides successful overall elastic property predictions and, more importantly sheds light on internal deformation behavior in the non-uniform microstructure of the woven laminates. The following points are noted:

1 Selection of representative volumes and boundary conditions are critical in evaluating deformation behavior of woven composite laminates. It is demonstrated that the difference between the upper and lower bound predictions for the effective properties may be significant. Mixed boundary conditions provide improved estimates of macroscopic stiffness over a wide range of weaving parameters when compared to previous models.

2 Due to three-dimensional anisotropy of the microstructure, the failure strength and mechanisms of woven laminates can be significantly different from those of the conventional laminates. The inherent imperfections in the woven laminate microstructure may cause additional complexities in failure modes and associated failure mechanisms. The current deformation model identifies dominant stress terms with regard to loading direction and weaving parameters.

3 Microscopic observations reveal that specimen fracture is the cumulative total of a series of nearly independent microstructural fracture events in the transverse, longitudinal and interlace regions. Depending on the loading type and laminate orientation, localized deformation in any one of these regions could govern failure of the laminate. For example, while a primary failure mechanism (failure of longitudinal fibers) predominates failure of the 0/90 laminates, under off-axes loading conditions damage accumulation in the matrix leads to failure of the laminate. These observations concur qualitatively with the stress quantities predicted by the deformation model.

4 The internal stresses, which may govern micro-failure mechanisms, are multiaxial even for uniaxial loading, as predicted by the deformation model. Development of general strength prediction methodologies for the woven laminate composites, therefore, requires understanding of the mechanics of each of these micro-failure mechanisms under multiaxial loading conditions. Due to microstructural complexity of the woven laminates, it was not possible to isolate a given parameter in a simple test as is the case with many monolithic materials. However, it is possible to devise tests where a given stress term and associated failure mechanism will dominate the failure.

5 The micromechanistic deformation model provides a unified constitutive equation which quantifies the relationships among the constituent properties, weaving parameters, and loading conditions. The description of micro- and macro-level deformation behavior with a constitutive equation would give insight into failure strength and associated failure mechanisms of the woven laminates. In the future, internal stress predic-

tions may be utilized to investigate mechanics of the micro-failure mechanisms and to construct failure envelopes for the transverse, longitudinal and interlace regions.

References

Agarwal, B. D., and Broutman, L. J., 1990, *Analysis and Performance of Fiber Composites*, Wiley, New York, NY.

Byun, J-H., and Chou, T-W., 1990, "Elastic Properties of Three-dimensional Angle-interlock Fabric Preforms," *Journal of Text. Inst.*, Vol. 81, pp. 538–548.

Byun, J-H., Whitney, T. J., and Du, G-W., and Chou, T-W., 1991, "Analytical Characterization of Two-Step Braided Composites," *Journal of Composite Materials*, Vol. 25, pp. 1599–1617.

Christensen, R. M., 1988, "Tensor Transformations and Failure Criteria for the Analysis of Fiber Composite Materials," *Journal of Composite Materials*, Vol. 22, pp. 874–897.

Chou, P. C., Carleone, J., and Hsu, C. M., 1972, "Elastic Constants of Layered Media," *Journal of Composite Materials*, Vol. 6, pp. 80–93.

Du, G. W., Chou, T-W., and Popper, P., 1991, "Analysis of Three-Dimensional Textile Preforms for Multidirectional Reinforcement of Composites," *Journal of Materials Science*, Vol. 26, pp. 3438–3448.

Ishikawa, T., 1981, "Anti-symmetric Elastic Properties of Composite Plates of Satin Weave Cloth," *Fibre Science and Technology*, Vol. 15, pp. 127–145.

Ishikawa, T., and Chou, T-W., 1983, "One-Dimensional Micromechanical Analysis of Woven Fabric Composites," *AIAA Journal*, Vol. 21, pp. 1714–1720.

Ishikawa, T., and Chou, T-W., 1982a, "Stiffness and Strength Behavior of Woven Fabric Composites," *Journal of Materials Science*, Vol. 17, pp. 3211–3220.

Ishikawa, T., and Chou, T-W., 1982b, "Elastic Behavior of Woven Hybrid Composites," *Journal of Composite Materials*, Vol. 16, pp. 2–19.

Jones, R. M., 1975, *Mechanics of Composite Materials*, Hemisphere Publication Corporation.

Ko, F. K., 1986, "Tensile Strength and Modulus of a Three-Dimensional Braid Composite," *Composite Materials: Testing and Design*, ASTM STP 893, J. M. Whitney, ed., pp. 392–403.

Love, A. E. H., 1944, *A Treatise on the Mathematical Theory of Elasticity*, 4th Edition, Dover Publications, New York.

Mirzadeh, F., and Reifsnider, K. L., 1992, "Micro-Deformations in C3000/PMR15 Woven Composite," *Journal of Composite Materials*, Vol. 26, pp. 185–205.

Naik, N. K., and Ganesh, V. K., 1992a, "Prediction of On-Axes Elastic Properties of Plain-Weave Fabric Composites," *Composites Science and Technology*, Vol. 45, pp. 135–152.

Naik, N. K., and Shembekar, P. S., 1992b, "Elastic Behavior of Woven Fabric Composites: I—Lamina Analysis," *Journal of Composites Materials*, Vol. 26, pp. 2196–2225.

Pagano, N. J., 1974, "Exact Moduli of Anisotropic Laminates," *Composite Materials*, L. J., Broutman and R. H. Krock, eds., *Mechanics of Composite Materials*, G. P. Sendeckyi, ed., New York, Academic Press, Vol. 2, pp. 23–44.

Postma, G. W., 1955, "Wave Propagation in a Stratified Medium," *Geophysics*, Vol. 20, pp. 780–806.

Shembekar, P. S., and Naik, N. K., 1992, "Elastic Behavior of Woven Fabric Composites: I—Laminate Analysis," *Journal of Composite Materials*, Vol. 26, pp. 2226–2246.

Sun, C. T., and Li, S., 1988, "Three-Dimensional Effective Elastic Constants for Thick Laminates," *Journal of Composite Materials*, Vol. 22, pp. 629–639.

Sun, C. T., and Liao, W. C., 1990, "Analysis of Thick Section Composite Laminates Using Effective Moduli," *Journal of Composite Materials*, Vol. 24, pp. 977–993.

Yang, J. N., Ma, C. L., and Chou, T. W., 1986, "Fiber Inclination Model of Three-Dimensional Textile Structural Composites," *Journal of Composite Materials*, Vol. 20, pp. 472–483.